Zoomorphology (2011) 130:147–166
DOI 10.1007/s00435-011-0128-x

ORIGINAL PAPER

Ultrastructure of spermatozoa in Orthalicidae (Mollusca, Gastropoda, Stylommatophora) and its systematic implications

María Gabriela Cuezzo

Received: 8 October 2010 / Revised: 12 May 2011 / Accepted: 19 May 2011 / Published online: 17 June 2011

Abstract Sperm morphology of orthalicid gastropods *Clessinia pagoda*, *Spixia tucumanensis*, *Plagiodontes daedaleus* (Odontostominae) and *Drymaeus hygrohylaeus*, *D. poecilus*, *Bostryx stelzneri* (Bulimulinae) are examined and described for the first time using transmission electron microscopy. Spermatozoa show the general characteristic of Pulmonata: an acrosomal vesicle, sperm nucleus helical, mitochondrial derivative forming a continuous sheath with paracrystalline material and coarse fibers associated with axonemal doublets. Features in the acrosomal complex and shape of the nucleus distinguish orthalicid sperms from other stylommatophoran. The acrosomal pedestal is traversed by fine striations in all species examined except in *S. tucumanensis*. The structure and thickness of the perinuclear sheath with a single or double layer of electron-dense material ensheathing the nuclear apex is characteristic of the group. The presence of a subnuclear ring in *Drymaeus*, *Bostryx* and *Clessinia* species is also reported. A data matrix of eleven species per 34 characters (16 sperm plus 18 anatomical and shell characters) from orthalicids plus other stylommatophoran and systellommatophoran representative species was constructed. Three cladistic analyses (sperm-based, anatomical-based and a combined sperm + anatomical-based) were performed to test the phylogenetic potential of sperm ultrastructure in orthalicid systematics and understand how sperm characters affect the topology and resolution of the obtained trees. Stylommatophora resulted in a monophyletic clade in the sperm-based and in the combined-character analysis. Orthalicidae is monophyletic only in the combined-character cladogram. Within Orthalicidae, Odontostominae is recovered as a monophyletic clade in all analyses, while Bulimulinae is paraphyletic in all trees except in the combined phylogeny. The present study and cladistic analyses performed support the hypothesis that characters on sperm ultrastructure are informative for stylommatophoran systematic and phylogenetic approaches, providing synapomorphies at familiar, subfamiliar and generic level.

Keywords Pulmonata · Odontostominae · Acrosome · Perinuclear sheath · Cladistics

Communicated by T. Bartolomaeus.

M. G. Cuezzo (✉)
CONICET-Facultad de Ciencias Naturales,
Universidad Nacional de Tucumán, Miguel Lillo 251,
4000 Tucumán, Argentina
e-mail: mcuezzo@unt.edu.ar

Introduction

Sperm morphology varies considerably within Gastropoda, particularly within the Caenogastropoda that produces typical and atypical sperms. Heterobranchia (Opisthobranchia + Pulmonata + several basal groups) gastropods produce only one type of sperm cells, a highly modified type, which is associated with internal fertilization (Franzén 1955; Maxwell 1983). Spermatozoa of pulmonates, like those of the rest of the heterobranch gastropods, rank among the most complex in the animal kingdom (Healy 2001). Studies on sperm morphology in Stylommatophora are relatively fewer in comparison with other molluscan groups. Some authors (Bayne 1970; Selmi et al. 1988. Giusti et al. 1991) considered that spermatozoa fine morphology in pulmonate gastropods is constant within families but provides limited clues regarding relationships between superfamilies. Moreover, Giusti et al. (1991)

stated that a large number of characters are constant in Stylommatophora such as the acrosomal structure and nucleus, with only one character suggesting an evolutionary trend from the lower to the higher stylommatophorans, the number of accessory helices in the midpiece. However, insufficient work has been conducted in Stylommatophora to make any relevant statement regarding the potential for sperm ultrastructure in systematics (Healy 1996, 2001). Most studies are non-comparative with no implication on the taxonomy or possible phylogeny for the mentioned groups. Although Helicoidea is the best-studied superfamily, the majority of the studies focus only on spermatogenesis and on parts of sperm structure (Anderson and Personne 1967; Takaichi and Sawada 1973; Takaichi and Dan 1977; Takaichi 1978; Dan and Takaichi 1979; Healy and Jamieson 1989; Giusti et al. 1991; Cuezzo 1994; Bojat et al. 2001). Chemical compartmentalization and different chemical aspects, especially in *Helix* spermatozoa, have also received abundant attention (Anderson et al. 1968; Anderson and Personne 1969a, b, 1970). Table 1 summarized published information on spermatozoa ultrastructure in stylommatophoran groups different from Helicoidea.

The Orthalicidae conform a large group of terrestrial pulmonates, mainly distributed in the Neotropical Region (Breure 1979). The genera *Spixia, Plagiodontes* and *Clessinia* have been classified within the traditional subfamily Odontostominae that has been recently considered a subgroup of Bulimulinae (Bouchet and Rocroi 2005). The genera *Bostryx* and *Drymaeus* belong to the Bulimulinae (Parodiz 1946; Breure 1979; Miquel 1993, 1995). The relationships among the genera of Odontostominae are unknown since no testable phylogeny has been proposed yet. Most of the genera within the Odontostominae are poorly defined, and their species composition is still unclear. *Clessinia* species for instance are endemics in central Argentina and share similar shell morphology with some *Spixia* species. Moreover, their geographical distribution is partially identical with some *Spixia* species (Parodiz 1942a, b; Salas Oroño 2007). The species that have been described within *Clessinia* are mostly known on the base of their shells and a single morphological character (shape of the aperture detached from the body whorl forming a cornet) separates them from *Spixia*. Almost complete absence of anatomical information and general shell similarities accordingly raised doubt on the monophyly of *Clessinia*. *Plagiodontes* is a well-defined genus of Odontostominae also mainly distributed in Argentina (Pizá 2008), although its phylogenetical affinities have not been established yet.

Bulimulinae species show a wider distribution area exceeding the Neotropical region, and the phylogenetic relationships within this group have been established in a previous cladistic analysis carried out by Breure (1979), Breure et al. (2010), and Cuezzo et al. (2010). In this sense, more data are available for Bulimulinae than for Odontostominae. *Drymaeus* species are usually arboreal, inhabiting humid tropical and subtropical forest, while *Bostryx* species are usually found in more xerophic habitats at higher altitudes (Miquel 1993, 1995). Previous research on sperm ultrastructure in Bulimulinae is restricted only to

Table 1 Published information on spermatozoa ultrastructure in stylommatophoran groups different from Helicoidea

Taxon	Genus/species	Bibliographic source
Achatinidae	*Achachatina marginata*	Odiete (1982)
	Achatina zebra	Whitehead and Hodgson (1985)
Agriolimacidae	*Agriolimax reticulatus*	Bayne (1970)
		Maxwell (1975)
Arionidae	*Arion hortensis*	Maxwell (1975)
Bradybaenidae	*Euhadra hickonis*	Takaichi (1975)
Discidae	*Discus rotundatus*	Maxwell (1976)
	Anguispira alternata	Atkinson (1982)
Limacidae	Limax *sp.*	Reger and Fitzgerald (1982)
Milacidae	*Milax sowerbyi*	Maxwell (1975)
Orthalicidae	*Scutalus tupacii*	Cuezzo (1995)
	Drymaeus hygrohylaeus	This study
	Drymaeus poecilus	This study
	Bostryx stelzneri	This study
	Plagiodontes daedaleus	This study
	Spixia tucumanensis	This study
	Clessinia pagoda	This study
Succineidae	*Oxyloma elegans*	Selmi et al. (1989)
	Succinea putris	Shileiko and Danilova (1979)

a single *Scutalus* species (Cuezzo 1995). Bulimulinae as well as the other subgroups of Orthalicidae have been alternatively classified as subfamilies or families of Orthalicoidea.

The aims of the present study are to examine sperm ultrastructure of species of both Odontostominae and Bulimulinae, providing new ultrastructural information, and to perform cladistic analyses using sperm characters to test their phylogenetical potential in orthalicid systematics, understanding how they affect the topology and resolution in the obtained hypotheses.

Materials and methods

Adult specimens from the Odontostominae species *Plagiodontes daedaleus* (Dehayes, 1820), *Spixia tucumanensis* (Parodiz, 1941), and *Clessinia pagoda* Hylton Scott, 1952, as well as from the Bulimulinae species *Drymaeus hygrohylaeus* (d'Orbigny, 1835), *D. poecilus* (d'Orbigny, 1835), and *Bostryx stelzneri* (Dorhn, 1875) were studied. These specimens were collected during summer, which is the land snail reproductive season. Voucher specimens are kept in the malacological collection of the Instituto Miguel Lillo (IML) of the Universidad Nacional de Tucumán, Tucumán, Argentina: IML 15339 A, *Plagiodontes daedaleus,* Tucumán Province, Trancas department, San Pedro de Colalao, S 26° 15′ 20" W 65° 30′ 23″, M. G. Cuezzo leg. IML 15336 A, *Spixia tucumanensis,* Tucumán Province, Trancas department, San Pedro de Colalao, on the road to Villa Rita, S 26° 15′ 20″ W 65° 30′ 23″, M.G. Cuezzo leg. IML 15237 A, *Clessinia pagoda,* Córdoba Province, Cruz del Eje department, San Marcos Sierra, Cerro de La Cruz, S 30° 47′ 22″ W 64° 37′ 96″, 677 m, February 16, 2006, M.G. Cuezzo & E. Salas Oroño leg. IML 15338 A, *Bostryx stelzneri,* Salta Province, Rosario de Lerma department, Route 52, Santa Rosa de Tastil, 3,200 m, December 28, 2007, M.G. Cuezzo leg. IML 15337 A, *Drymaeus hygrohylaeus,* Salta Province, Anta department, El Rey Nacional Park, Maldonado mountain, S 24° 43′ 27″ W 64° 38′ 46″, 1,200 m, M.G. Cuezzo leg. IML 15397 A, *Drymaeus poecilus,* Tucumán Province, Capital department, San Miguel de Tucumán, S 26° 49′ 09.43″ W 65° 14′ 32.83″, 450 m, M.G. Cuezzo leg.

Hermaphroditic ducts and seminal vesicles were dissected and small portions fixed in Karnovsky's solution (Karnovsky 1965) at 4°C with 0.1 M phosphate buffer (pH 7.2) and post-fixed overnight in 2% osmium tetroxide in phosphate buffer. The tissue was rinsed several times in phosphate buffer solution, dehydrated in a series of alcohol and embedded in Epon-Araldite resin. Ultrathin sections obtained with a Reichert ultramicrotome were collected on 200-μm mesh copper grids and routinely stained with 2% uranyl acetate in 0.1 M phosphate buffer for 2 h at 4°C. A second stain lead citrate was also applied, as usually done to obtain a good contrast. Later grids were examined in a Zeiss EM 109 Electron Microscope at LAMENOA (Electron microscopy laboratory of the Universidad Nacional de Tucumán-CONICET).

Cladistic analysis

Taxon selection, characters, and codings

A data matrix consisting of eleven species and sixteen sperm characters was compiled to test the phylogenetic signal in sperm ultrastructure for orthalicid systematics. Eighteen other morphological characters from the shell, pallial, and reproductive systems of the same taxa were added to the original sperm-based matrix. Combined matrix of the total number of sperm and anatomical characters is illustrated in Table 2.

The ingroup taxa in the matrix consists of the currently studied orthalicoidean species and three other stylommatophoran with known sperm morphology (*Epiphragmophora tucumanensis* (Doering, 1874), *Cornu aspersum* (Müller, 1774) (= *Helix aspersa, Cantareus aspersum*), and *Scutalus tupacii* (d'Orbigny, 1835). Three Systellommatophora species (*Phyllocaulis soleiformis* (d'Orbigny, 1835) (= *Vaginulus borellianus* (Colosi, 1921)), *Onchidella celticum* (Cuvier, 1817), and *Onchidium damelii* Semper, 1885) were used as outgroups. Species included in the matrix represent two main stylommatophoran groups: Helicoidea (Helicidae, Epiphragmophoridae) and Orthalicoidea (Odontostominae and Bulimulinae) and two main systellommatophoran taxa: Veronicelloidea (Veronicellidae) and Onchidioidea: (Onchidiidae) (Table 2). Sperm characters coded for Onchiididae, Veronicellidae, Epiphragmophoridae, and Helicidae are based on published data (Lanza and Quattrini 1964; Quattrini and Lanza 1965; Healy 1986, Selmi et al. 1988; Healy and Jamieson 1989; Cuezzo 1994). Similarly, anatomical characters coded for these taxa are based on published information (Barker 2001; Cuezzo 2006; Rodrigues Gomes 2007; Dayrat 2010). Anatomical characters coded for Orthalicidae were extracted from Cuezzo et al. (2010) cladistic analysis. Nevertheless, due to the different taxonomic coverage of the present study, some characters used in Cuezzo et al. (2010) were here omitted as they were not informative for the smaller set of taxa in this analysis. Anatomical characters coded for Onchidiidae are based on *Onchidium vaigiense* Quoy and Gaimard, 1824 (Dayrat 2010). Onchidiidae is listed at family level because anatomical information was not available for the species with known sperm morphology (*O. damelii* and *O. celticum*). For this

Table 2 Data matrix for the characters (1–34) and taxa (11) (orthalicids + other stylommatophoran and systellommatophoran species) used in this study

Taxa/characters	0 1	0 2	00 34	00000 56789	111 012	1111111 3456789	2222222222 0123456789	33333 01234
Onchidiidae	3−4	0.87	0[02]	0???0	00[01]	0110?0?	??11?0?00[01]	????0
Phyllocaulis soleiformis	?	0.4−0.6	10	0???0	001	???1?0?	??01100000	????0
Cornu aspersum	8.1	0.33	00	10100	000	1000201	0210100111	00001
Epiphragmophora tucumanensis	8.1	0.5	00	10100	000	1000201	0101200111	00001
Scutalus tupacii	7.5	0.13	11	10100	000	1000100	1011010011	11000
Bostryx stelzneri	5.5	0.33	11	10110	010	1000000	1111010011	11000
Drymaeus hygrohylaeus	9.6	0.3	11	10110	010	1000100	1100000011	11000
Drymaeus poecilus	9.5	0.3	11	10110	010	1000100	1100000011	11000
Clessinia pagoda	6.4	0.1	11	11011	110	1000211	1000201011	21110
Spixia tucumanensis	5.75	0.15	10	11011	100	1000211	1000101011	21110
Plagiodontes daedaleus	5.2	0.15−0.2	11	10011	100	1000311	1010101011	11100

Sperm characters (1–16), anatomical and shell characters (17–34). ? = missing characters

reason, information was obtained from other related species (*O. vaigiense*) of the same family following methodology applied by Ponder and Lindberg (1997).

A list of all characters used in the data matrix is presented in Table 3. Character coding follows Sereno (2007). From a total number of 34 characters used, four are multistate and the rest are binary. The first two characters in the matrix are continuous and are treated as additive. The rest of the characters are treated as unordered (non-additive). Missing or inapplicable characters are assigned a "?" entry.

Although sperm morphology of other stylommatophoran groups is known, the available data are difficult to compare or sperms have been only partially described. For this reason, only ultrastructural studies of whole sperms were considered for character coding. Due to the scarce taxon representation, this cladistic analysis is carried out only to test the value of sperm characters to use in future cladistic analysis.

Phylogenetic analysis

Three cladistic analyses were performed: (1) using sperm characters alone, (2) using anatomical + shell characters alone and (3) combining sperm and anatomical + shell characters to test character congruence and understand how sperm characters affect the topology and resolution of the most parsimonious trees obtained in the analyses performed.

Trees obtained were rooted in Onchidiidae and alternatively in *Phyllocaulis soleiformis.* Computer program TNT (Goloboff et al. 2008) for parsimony analysis was used to obtain the phylogenetic hypotheses presented herein (Figs. 7, 8, 9). TNT analyses were performed under implicit enumeration collapsing zero-length branches, an exact solution using branch-and-bound applied to small data sets that guarantee finding all optimal trees under current settings. This usually is sufficient for all global optima ("islands") to be found.

Common synapomorphies were mapped on the obtained trees illustrated in each case using WINCLADA (Nixon 1999). Information on character changes in each node was also obtained using TNT.

Group support estimation

Bremer support (Bremer 1988, 1994) indicating clade support was calculated. Under IW, 10,000 most parsimonious trees and 10,000 suboptimal trees up to 10 units of fit below the optimal trees were gathered (by TBR swapping from optimal trees). Suboptimal trees were gathered in consecutive stages, saving at each stage 1,000 trees and making the suboptimal trees worse by 0.1, 0.2, 0.3, 0.5, 1, 2, 3, 5, 8, and 10 units of fit (this stepwise search allows a more accurate estimation of the supports).

Results

In the present study, autosperm of Odontostominae and Bulimulinae species of the Orthalicidae (= Bulimulidae) isolated from the seminal vesicle (hermaphroditic duct) were examined. The spermatozoon of the studied species exhibits a long head formed by the acrosomal complex, nucleus and perinuclear sheath with a long midpiece

Table 3 List of characters and character states used and codified in the matrix

Character	Character state and codification
1. Sperm head, nucleus length:	Continuous (3–9.6 μm)
2. Acrosome, pedestal length, relative to vesicle length:	Continuous (0.1–0.87 μm)
3. Acrosome, vesicle, shape:	(0) round; (1) oval
4. Acrosome, pedestal, substructure:	(0) granular homogeneous; (1) irregular fine striations
5. Nucleus, perinuclear sheath:	(0) absent; (1) present
6. Nucleus, perinuclear sheath, substructure:	(0) moderate electron-dense granules; (1) highly electron-dense granules
7. Nucleus, perinuclear sheath, thickness:	(0) thick; (1) thin
8. Nucleus, perinuclear sheath, internal cap, number:	(0) single layer; (1) double layer
9. Nucleus tip, width relative to pedestal width:	(0) equal or narrower; (1) wider
10. Nucleus, nuclear keels, extent of projections relative to nuclear outline:	(0) slightly pronounced keels; (1) moderately pronounced only at nuclear base
11. Nucleus/midpiece, subnuclear ring:	(0) absent; (1) present
12. Midpiece, glycogen helices, maximum number:	(0) one; (1) more than one
13. Midpiece, axoneme:	(0) continuous along midpiece; (1) terminates within midpiece, in its posterior region
14. Midpiece, annulus:	(0) absent; (1) present
15. Midpiece, glycogen piece:	(0) absent; (1) present
16. Midpiece, secondary helices:	(0) absent; (1) present
17. Pallial system, secondary ureter, opening in relation to pulmonary roof:	(0) open at midportion; (1) open at distal portion before reaching mantle collar; (2) totally closed and opening at mantle collar; (3) open at proximal portion
18. Pallial complex, pallial gland parallel to mantle collar:	(0) absent; (1) present
19. Reproductive system, epiphallus, length in relation to penis:	(0) longer than penis; (1) shorter than penis
20. Reproductive system, Vas deferens in relation to penial sheath:	(0) no relation; (1) vas deferens runs under penial sheath
21. Reproductive system, penis sheath, degree of overlap:	(0) basal short cuff-like; (1) overlapping part of penis but not cuff-like; (2) overlapping complete penis length
22. Penis, verge:	(0) absent; (1) present
23. Reproductive system, bursa copulatrix duct:	(0) longer than spermoviduct; (1) shorter
24. Reproductive system, penial muscle, insertion on penial complex:	(0) terminal, on flagellum; (1) lateral on epiphallus; (2) lateral on penis
25. Reproductive system, constriction in penis:	(0) absent; (1) present
26. Reproductive system, epiphallus, epiphallic papilla:	(0) absent; (1) present
27. Terminal genitalia, accessory glands in female portion:	(0) absent; (1) present
28. Genital openings:	(0) separated; (1) fused
29. External morphology, eye position:	(0) at tip of retractile but not evaginable tentacle; (1) at tip of elongate, retractile and evaginable tentacle
30. Shell, general shape, longitudinal axis respect to body whorl width:	(0) heliciform, longitudinal axis shorter than body whorl width; (1) oval-oblong, longitudinal axis length close to double the body whorl width; (2) fusiform to turriteliform, longitudinal axis length more than twice the body whorl width
31. Shell, protoconch:	(0) smooth; (1) sculptured
32. Shell, presence of teeth or lamella in the aperture:	(0) absent; (1) present
33. Shell, periostracal structures:	(0) absent; (1) present
34. Terminal genitalia, dart sac:	(0) absent (0); present (1)

forming the "spermatozoon tail" that is inserted in the nuclear implantation fossa at the base of the nucleus.

Bostryx stelzneri (Dohrn, 1875) (Bulimulinae)

Acrosomal complex

The acrosome consists of an oval membrane-bound vesicle (0.3 μm in length and 0.2 μm in diameter) set on a shallow anterior depression of the acrosomal pedestal (Fig. 1a). The basal side of the vesicle is convex, adjusting to the concave apical shape of the pedestal. The internal content of the vesicle is homogeneously electron-dense. The pedestal is cylindrical with 0.33 μm in length and 0.18 μm in diameter traversed by an array of fine striations from side to side with electron-lucent spaces between them. A perinuclear sheath encloses the pedestal and an apical portion of the nucleus. This sheath is formed by granular, scatter, moderately electron-dense material, and the degree in which it encloses the nucleus varies depending on the level of the section (Fig. 1b, c). Embedded in this granular material a short and more electron-dense layer is visible at the apical portion of the nucleus (Fig. 1a). In longitudinal sections, the perinuclear sheath encloses the anterior half of the nucleus on one side, while on the other side, it is much shorter lining less than one half of the nuclear membrane. Transversal sections show that the most complete enclosure of the nucleus occurs near the nuclear apex (Fig. 1a, b). Lower levels of the nucleus sections show the perinuclear sheath lining on less than half of the nuclear diameter.

Nucleus

The nucleus is long and slender and slightly helically coiled, 5.5 μm in length and 1.2–1.4 μm in diameter at the base, and measures 0.15 μm (at the level of indentation) to 0.24 μm (posterior to the nuclear indentation) in width at the apex. It is basally invaginated forming the implantation fossa where the midpiece is inserted. The nuclear chromatin is homogeneously condensed, and few electron-lucent areas are visible especially in the basal portion of the nucleus. The apical portion of the nucleus shows a lateral notch distinguishable on longitudinal sections (Fig. 1a). A subnuclear rig is clearly visible at the base of the nucleus (Fig. 1g).

Midpiece

The nuclear implantation fossa is filled with the centriolar derivative, which is distally continued by a circular array of nine coarse fibers that accompany the axonemal doublets throughout most of the midpiece. The coarse fibers plus the axonemal doublets together with the two central microtubules conform a $9 + 2 + 9$ configuration of the axoneme (Figs. 1d–g, 6a–c) clearly visible in transversal sections. In the proximal portion of the midpiece, the coarse fibers are thick and periodically banded (1 g). The peripheral doublets of the axoneme are embedded and masked by the coarse fibers at the implantation fossa (Figs. 1d, e, 6a, b), emerging at the beginning of the glycogen helix region of the midpiece (Fig. 1h). A granular distal accessory sheath surrounds the central microtubules (Fig. 1g). Along the midpiece, the axoneme and coarse fibers are surrounded by matrix and paracrystalline material of the mitochondrial derivative. Initially, the coarse fibers enclosing the axonemal doublets are surrounded by paracrystalline material only (Fig. 1f, g). Further posterior, the coarse fibers and emergent axonemal doublets are surrounded by either one or two rows of matrix material and also paracrystalline material of the mitochondrial derivative (Fig. 1g, h). A single helix runs through the mitochondrial derivative that is occupied by glycogen-like granules; membranous material (Fig. 1g, h, i) is also present. Along the midpiece, the size and shape of the helix decrease considerably, gradually reducing the number of glycogen-like granules until the helix disappears. The terminal portion of the midpiece begins with the loss of the two central axonemal tubules and coarse fibers followed by the loss of the helix (Fig. 1i). The space occupied by the axoneme and coarse fibers is filled by dense granules and membranous deposits (Fig. 1j, k). Terminal portion of the midpiece is composed by paracrystalline material.

Drymaeus hygrohylaeus (d'Orbigny, 1835) and *D. poecilus* (d'Orbigny, 1835) (Bulimulinae)

Acrosomal complex

In both species, the acrosomal complex is identically organized. The acrosome consists of an oval membrane-bound vesicle (0.2 μm in diameter and 0.3 μm in length) set on an anterior depression of the acrosomal pedestal (Fig. 2a). The basal side of the vesicle is convex, adjusting to the concave apical shape of the pedestal. The internal content of the vesicle is homogeneously electron-dense. An acrosomal pedestal that connects the tip of the nucleus with the acrosomal vesicle is present. The pedestal is cylindrical with 0.3 μm in length and 0.15–0.2 μm in diameter traversed by thin striations from side to side. An electron-lucent cylindrical middle area is clearly distinguished in the pedestal area (Fig. 2b). In some sperms, the acrosome is tilted at an angle with respect to the longitudinal axis of the nucleus (Fig. 2b, c). A perinuclear sheath encloses the pedestal and a portion of the nucleus (Fig. 2a, b) formed by an electron-dense layer embedded in granular, less electron-dense material Fig. 2b). The degree in which the

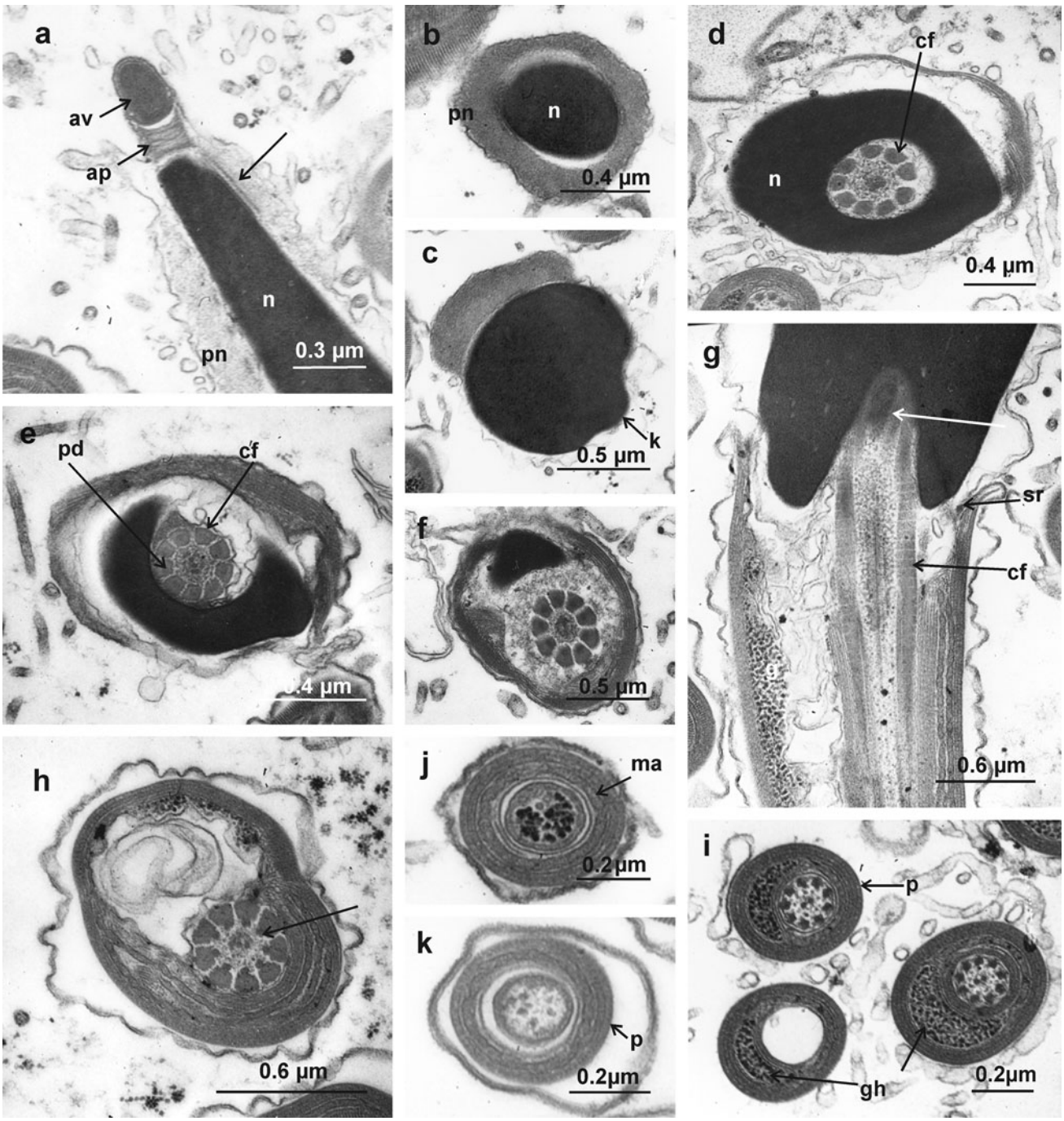

Fig. 1 *Bostryx stelzneri*, **a** Longitudinal section (LS) of acrosomal complex set on the nuclear tip. Note the thin striations across the acrosomal pedestal. *Arrow* shows the layer of electron-dense material embedded in the perinuclear sheath. **b** Transverse section (TS) through nucleus surrounded by perinuclear sheath. **c** TS through nucleus partially overlapped by terminal portion of perinuclear sheath. A keel is clearly visible in the nuclear section. **d** TS of basal nucleus level with implantation fossa. **e** TS through implantation fossa. Peripheral doublets of axoneme are embedded into a circular array of nine coarse fibers that accompany the central axonemal doublets. **f** TS of last portion of nucleus level with proximal midpiece. **g** LS through distal nucleus and proximal midpiece. Note the thick coarse fibers that are periodically banded. *Arrow* points toward the basal body located in the implantation fossa. **h** TS through proximal midpiece or "neck region". *Arrow* points to the peripheral doublets of the axoneme emerging from the coarse fibers. **i** TS of midpiece at different levels showing the glycogen helix. **j–k** TS of midpiece. The axoneme is replaced by granular material ensheathed by the mitochondrial derivative. *av* acrosomal vesicle, *ap* acrosomal pedestal, *cf* coarse fibers, *g* glycogen-like granules, *gh* glycogen helix, *k* nuclear keel, *ma* matrix material of the mitochondrial derivative, *n* nucleus, *p* paracrystalline material, *pd* peripheral doublets, *pn* perinuclear sheath, *sr* subnuclear ring

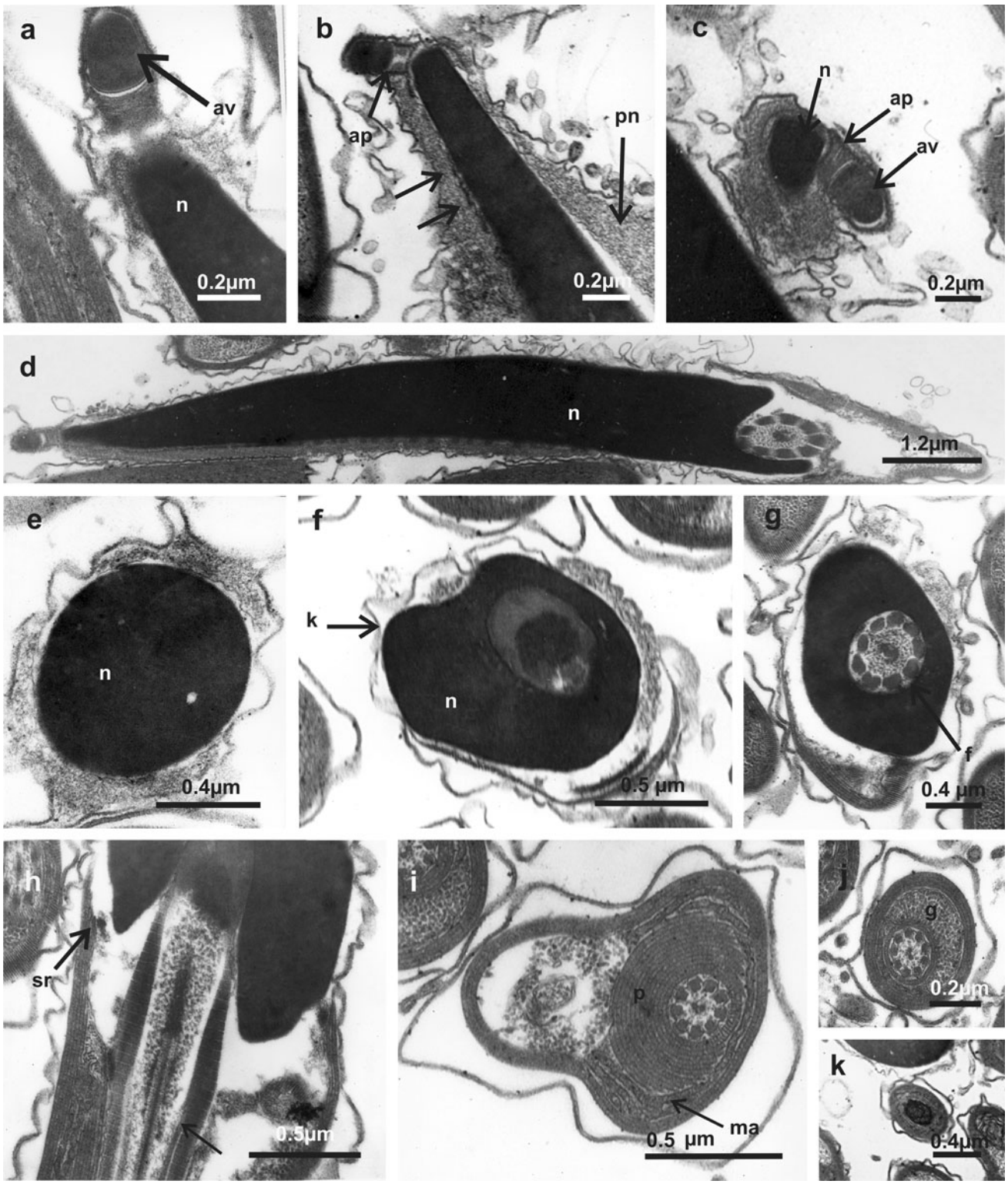

perinuclear sheath encloses the nucleus varies depending on the level of the section (Fig. 2b–e). In longitudinal sections, the perinuclear sheath encloses three quarters of the nucleus on one side, while on the other side, there is a much shorter lining of less than one half of the nuclear membrane (Fig. 2d). Lower levels of the nucleus sections show perinuclear sheath lining on less than half of the nuclear diameter.

◀ **Fig. 2** *Drymaeus hygrohylaeus,* **a** Longitudinal section (LS) of acrosomal complex and nuclear tip. **b** LS of the proximal nucleus with acrosome tilted, note the transverse striation of the pedestal. **c** Detail of an acrosomal tilted at a higher angle with respect to the nucleus. *Arrows* highlight the presence of an electron-dense layer inside perinuclear sheath. **d** LS of a complete head showing nucleus shape and acrosome strength with respect to the nuclear axis. **e** TS of nucleus with distal portion of perinuclear sheath. **f** TS of nucleus at the level of the implantation fossa with basal body. Note nuclear keels. **g** TS of nucleus with distal portion of implantation fossa. **h** LS of nucleus/midpiece junction. *Arrow* shows the emergence of axonemal doublets from coarse fibers. **i** TS of midpiece at the level of glycogen helix. Note the layers of paracrystalline material of the mitochondrial derivative surrounding the axoneme. **j** TS of midpiece with glycogen helix with reduced layers of paracrystalline layers. **k** TS of midpiece, the space formerly occupied by the axoneme is now full of granular and membranous material. *av* acrosomal vesicle, *ap* acrosomal pedestal, *f* implantation fossa, *g* glycogen-like granules, *k* nuclear keel, *ma* matrix material, *n* nucleus, *p* paracrystalline material, *pn* perinuclear sheath, *sr* subnuclear ring

Nucleus

In both species, the nucleus is long and slender (Fig. 2a–d), 9.96 μm in length, 1.18–1.47 μm in diameter at the base and 0.2–0.3 μm at the tip, slightly helically coiled. The nucleus is basally invaginated, forming the implantation fossa where the midpiece is inserted (Fig. 2e–g). The nuclear chromatin is homogeneously condensed, with scatter electron-lucent areas visible. The apical portion of the nucleus shows a lateral small indentation clearly visible on longitudinal sections (Fig. 2b). A subnuclear rig is distinguished at the base of the nucleus (Fig. 2h).

Midpiece

The morphology of the midpiece in both species corresponds to the previous description for *Bostryx stelzneri* (Fig. 2h–k). The nuclear implantation fossa is filled with the centriolar derivative (Fig. 2f, h), which is distally continued by a circular array of nine coarse fibers (Fig. 2g, h) that accompany the axonemal doublets throughout most of the midpiece. The coarse fibers, the axonemal doublets, and the two central microtubules form the 9 + 2 + 9 pattern of the axoneme (Fig. 2f–h). A single glycogen helix runs along the midpiece ensheathed by matrix and paracrystalline mitochondrial derivative that progressively diminished its size toward the terminal midpiece (Fig. 2i, j). In terminal portion of the midpiece, the two central axonemal tubules and coarse fibers disappear at first, followed by the helix. The space occupied by the axoneme and coarse fibers is filled by dense granules and membranous deposits (Fig. 2k).

Clessinia pagoda Hylton Scott, 1952 (Odontostominae)

Acrosomal complex

The acrosome consists of an oval membrane-bound vesicle (0.4 μm in length and 0.3 μm in diameter) with shallow curved base forming a semicircle that is set on the acrosomal pedestal (Fig. 3a, b). The vesicle is fulfilled with granular, homogeneous material. The acrosomal pedestal is shallow and cylindrical with 0.1 μm in length and 0.3 μm in width with fine parallel striation. A clear space is located between the vesicle and the pedestal (Fig. 3b). A perinuclear sheath encloses one side of the pedestal and the apical portion of the nucleus. The perinuclear sheath is very short in length, overlapping only a small apical portion of the nucleus. This sheath consists of a layer of electron-dense material that forms a cap in the nuclear apex which is embedded into granular, electron-lucent scattered material (Fig. 3a–c).

Nucleus

The nucleus is thick and helically coiled, 6.4 μm in length, 1.2 μm in width at the base, and about 0.4 μm width at the apex (Fig. 3a–d). It is wider in its middle portion (1.9–2.0 μm) and decreases in width toward its basal portion (1.2–1.3 μm). The nucleus is basally invaginated forming the implantation fossa where the midpiece is inserted (Fig. 3e). The nuclear chromatin is homogeneously condensed with no electron-lucent areas visible. A subnuclear rig is clearly visible at the base of the nucleus (Fig. 3e).

Midpiece

The nuclear implantation fossa is filled with the centriolar derivative that is distally continued by a circular array of nine coarse fibers that accompany the axonemal doublets throughout most of the midpiece (Fig. 3e). Coarse fibers, axonemal doublets, and the two central microtubules cause the 9 + 2 + 9 pattern of the axoneme (Fig. 6a–c). In the proximal portion of the midpiece, the coarse fibers are thick and periodically banded. The peripheral doublets of the axoneme are embedded and masked by the coarse fibers at the implantation fossa, emerging at the beginning of the glycogen helix region of the midpiece (Fig. 6b). A granular distal accessory sheath surrounds the central microtubules. Along the midpiece, the axoneme and coarse fibers are surrounded by matrix and paracrystalline material of the mitochondrial derivative (Fig. 3e, f). Initially, the coarse fibers enclosing the axonemal doublets are surrounded only by paracrystalline material (Fig. 3e). Further posterior, the

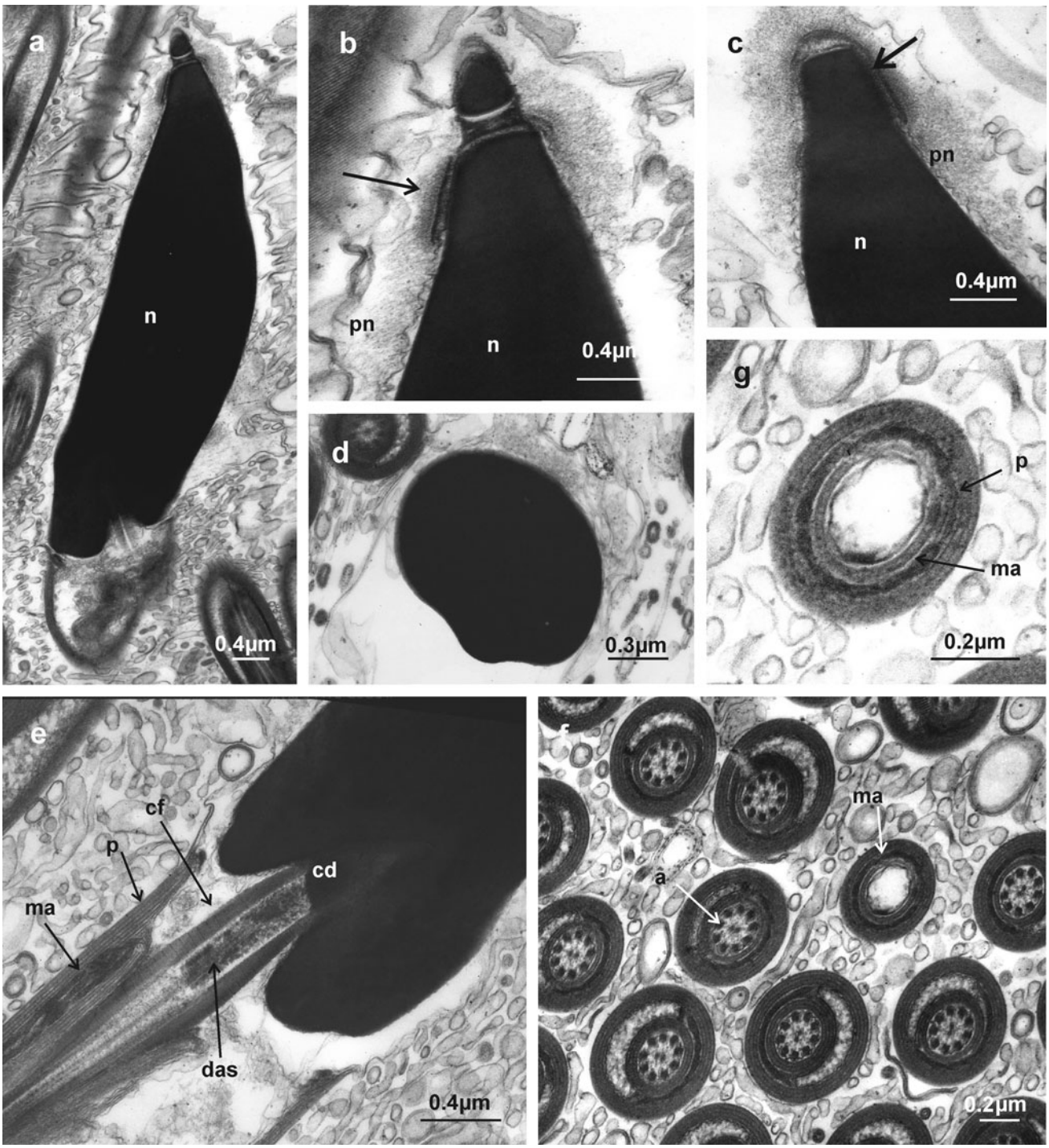

Fig. 3 *Clessinia pagoda,* **a** Longitudinal section (LS) of nucleus and acrosomal complex. Note the particular nuclear shape thicker in its median portion. **b** Detail of the acrosomal complex; *arrow* points to the electron-dense layer embedded into the perinuclear sheath. Note the acrosomal pedestal wider than taller. **c** Nuclear tip surrounded by perinuclear sheath; *arrow* points to the nuclear cap. **d** Transverse section (TS) of nucleus showing a keel. **e** LS of nucleus/midpiece junction showing basal invagination of nucleus. The axoneme plus the banded coarse fibers are surrounded by matrix and paracrystalline material of the mitochondrial derivative. **f** TS through midpiece at different levels. Note single glycogen helix and single matrix layer. Section showing absence of axoneme. **g** Detail of posterior section of midpiece where axoneme is lost. *a* axoneme, *cd* centriolar derivative, *cf* coarse fibers, *das* distal accessory sheath, *ma* matrix material, *n* nucleus, *p* paracrystalline material of the mitochondrial derivative, and *pn* perinuclear sheath

coarse fibers and emergent axonemal doublets are surrounded by three to one rows of matrix material and also several paracrystalline material of the mitochondrial derivative. A single helix runs through the mitochondrial derivative (Fig. 3f, g) that is occupied by glycogen-like granules and membranous material. Along the midpiece, the size and shape of the helix decrease considerably by gradually reducing its contents of glycogen-like granules until it disappears (Fig. 6b–f). In the terminal portion of the midpiece, the two central axonemal tubules and coarse fibers disappear at first (Fig. 3g), followed by the helix. Finally, the layer of matrix material of the mitochondrial derivative also disappears and only a thin double layer of paracrystalline material remains (Fig. 6e–f). The diameter of the midpiece in this portion is clearly reduced.

Spixia tucumanensis (Parodiz, 1941) (Odontostominae)

Acrosomal complex

The acrosome consists of an oval membrane-bound vesicle with shallow curved base forming a semicircle that is set on the acrosomal pedestal (Fig. 4a, b). The vesicle (0.3 μm in length and 0.2 μm in diameter) is fulfilled with electron-dense material. The acrosomal pedestal is shallow, cylindrical, with 0.15 μm in length and 0.2 μm in width, with no fine striation evident. No clear space is seen between the vesicle and the pedestal and the vesicle rest on the pedestal. A thick perinuclear sheath encloses one side of the pedestal and the apical to medial portion of the nucleus (Fig. 4a–c). This sheath is formed by granular, electron-dense material with a dark and homogeneous appearance interposed between the nucleus and the plasma membrane. The perinuclear sheath is long enclosing the anterior half of the nucleus on one side, while on the other side, there is a much shorter lining of less than one half of the nuclear membrane (Fig. 4a). Transversal sections show that the most complete enclosure of nucleus occurs near the nuclear apex (Fig. 4d). Immersed in the perinuclear sheath, a dark layer forming a hood on the apical nucleus can clearly be distinguished, especially in longitudinal sections (Fig. 4b, c). This layer is continuous in the apical portion forming a cap and is interrupted by electron-lucent spaces in the longer side of the perinuclear sheath forming semicircular rings overlapping one side of the nucleus (Fig. 4b). In transversal sections of the apical portion of the nucleus, this layer is continuous (Fig. 4c).

Nucleus

The nucleus is thick especially in its basal portion, 5.75 μm in length, 0.3 at its tip, 1.30–140 μm width in the median portion, and 1.46–1.52 μm in width at the base, helically coiled (Fig. 4a). Its general shape is triangular wider at the distal portion. It is basally invaginated forming the implantation fossa where the midpiece is inserted (Fig. 4e, g). The nuclear chromatin is homogeneously condensed with no electron-lucent areas visible. The implantation fossa (Fig. 4g) shows no variation from the above description for *Clessinia pagoda.*

Midpiece

The midpiece (Fig. 4f–i) shows the same structure described for *Clessinia pagoda.*

Plagiodontes daedaleus (Deshayes, 1820) (Odontostominae)

Acrosomal complex

The acrosome consists of an oval membrane-bound vesicle with shallow curved base forming a semicircle that is set on a shallow depression of the acrosomal pedestal (Fig. 5a, b). The acrosomal vesicle length is 0.31–0.35 μm and is fulfilled with homogeneous electron-dense material. The acrosomal pedestal is cylindrical with a maximum length of 0.2 μm in the borders and of 0.15 μm in the middle and 0.2–0.3 μm in width, traversed by an array of thin striations interrupted in the middle zone by a clear area. Electron-lucent spaces between them are distinguished (Fig. 5b). A clear space is seen between the acrosomal vesicle and the upper portion of the acrosomal pedestal. A perinuclear sheath encloses one side of the pedestal and the apical portion of the nucleus (Fig. 5a–d). This sheath is formed by granular, moderate electron-dense material with granulose appearance. The perinuclear sheath is short, enclosing the anterior apical portion of the nucleus on one side, while it is much shorter on the other side (Fig. 5a, b). A double, continuous layer parallel to the nuclear membrane is embedded in the granular material of the perinuclear sheath. The inner layer is more conspicuous than the outer layer (Fig. 5b). Both layers form a hood covering the nucleus apically (Fig. 5b, c).

Nucleus

The nucleus is thick, helically coiled along its length, 5.2 μm in length, with a maximum diameter of 1.45–1.50 μm and 1.2 μm width at the base. The apical portion of the nucleus 0.3–0.4 μm in width is convex,

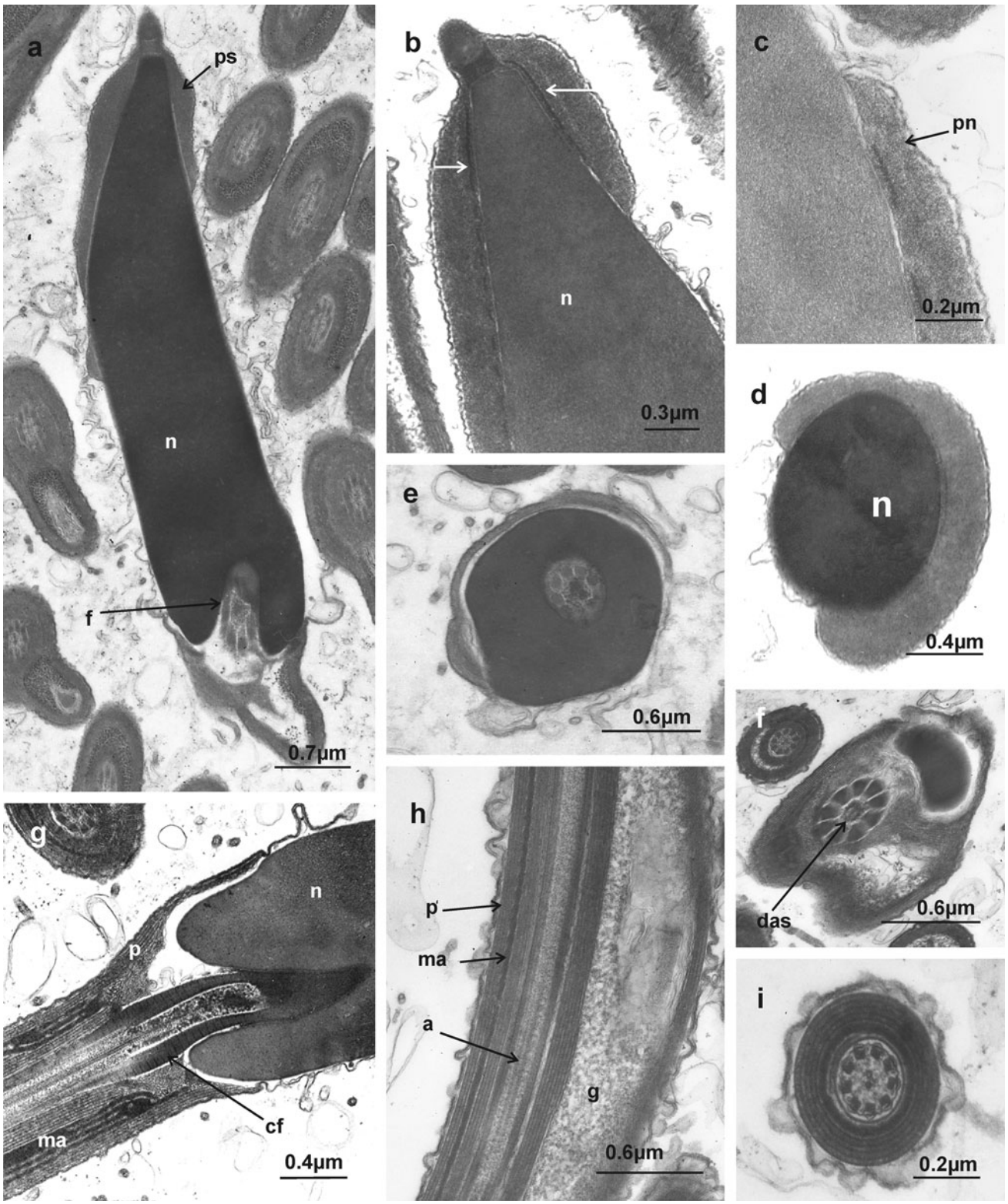

showing a clear space that separates the nuclear apex from the acrosomal pedestal (Fig. 5a, b). The chromatin is homogeneously condensed with no electron-lucent areas visible along the nucleus (Fig. 5d, e).The nucleus is basally invaginated, forming the implantation fossa where the midpiece is inserted.

◀ **Fig. 4** *Spixia tucumanensis,* **a** Longitudinal section (LS) of a sperm head showing acrosomal complex and nucleus. **b** Detail of nuclear apex and acrosomal complex. *Arrow* points the perinuclear electron-dense layers embedded into a thicker granular sheath. **c** Detail of the electron-dense layer interrupted by electron-lucent spaces inside perinuclear sheath. *Arrows* indicate electron-dense layer. **d** Transverse section (TS) of nucleus surrounded by the thick and electron-dense perinuclear sheath. **e** TS of nucleus at the level of the implantation fossa. The nucleus is surrounded by paracrystalline material of the mitochondrial derivative. Note the granular distal accessory sheath surrounding the central doublets of the axoneme. **f** Posterior TS of nucleus/midpiece junction. A small distal portion of the nucleus is visible. **g** LS of nucleus/midpiece junction. **h** LS of midpiece showing the axoneme plus coarse fibers surrounded by a single layer of matrix material and several layers of paracrystalline material of mitochondrial derivative. The midpiece is traverse by a glycogen helix with glycogen-like granules and membranous material. **i** TS of midpiece without glycogen helix. *a* axoneme, *n* nucleus, *pn* perinuclear sheath, *cf* coarse fibers, *das* distal accessory sheath, *f* implantation fossa, *g* glycogen-like granules, *ma* matrix material, *p* paracrystalline material of mitochondrial derivative

Midpiece

The morphology of the midpiece is similar to the previous species described. Along the midpiece, the axoneme and coarse fibers are surrounded by matrix and paracrystalline material of the mitochondrial derivative. A single helix runs through the mitochondrial derivative, which close to the implantation fossa is occupied by the membranous material (Fig. 5f) and posteriorly by glycogen-like granules (Fig. 5g, h). Along the midpiece, the size and shape of the helix decrease considerably by gradually reducing its contents of glycogen-like granules until it disappears. The terminal portion of the midpiece is formed by layers of the mitochondrial derivative with its inner space being filled with membranous material. Transverse sections reveal that the posteriormost portion of midpiece is formed by a thin layer of paracrystalline mitochondrial derivative with an empty central space (Figs. 5i, 6).

Cladistic analysis

The results from the analysis on the different sets of characters are as follows:

(1) Sperm characters alone (characters 1–16, Table 2). One tree was obtained, with a length of 27 steps (Fig. 7).
(2) Anatomical + shell characters alone (characters 17–34, Table 2). Four trees were obtained. Strict consensus tree with a length of 28 steps (Fig. 8).
(3) Sperms, anatomical + shell characters (characters 1–34, Table 2). One tree was obtained, with a length of 60 steps (Fig. 9).

In two analyses performed, *Phyllocaulis soleiformis* (= *Vaginulus borellianus*) is basal and sister group of the "stylommatophoran clade" (Figs. 7, 9). When only sperms are considered (Fig. 7), the monophyly of the stylommatophoran clade (node 17, Bremer support score = 1) is sustained by three synapomorphies: acrosomal pedestal length [2(0.6)], acrosomal pedestal substructure [4(1)], and presence of perinuclear sheath [5(1)]. Orthalicidae and Bulimulinae are paraphyletic in the tree obtained from the sperm-based matrix. On the contrary, Odontostominae represented by *Plagiodontes daedaleus, Spixia tucumanensis,* and *Clessinia pagoda* (node 20) is monophyletic with a good Bremer support score (1.4). Sperm synapomorphies for Odontostominae are acrosomal pedestal length [2(0.2)]), thick perinuclear sheath [7(0)], nucleus tip wider than pedestal [9(1)], and nuclear keels evident at nuclear base [10(1)]. The helicoidean clade represented by *Epiphragmophora tucumanensis* and *Cornu aspersum* is merged with Bulimulinae species. The helicoidean clade is supported in the sperm-based analysis (Fig. 7, node 13, Bremer support value = 1.4) by three synapomorphies: acrosomal pedestal length [2(0.33)], round acrosomal vesicle [3(0)], and granular acrosomal pedestal substructure [4(0)].

When the cladistic analysis was performed using only anatomical + shell characters (Fig. 8), Orthalicidae and Bulimulinae are paraphyletic while Odontostominae is recovered as a monophyletic clade (node 16, Bremer support score = 2). There is no resolution on the relationships between helicoidean (node 13) and orthalicids. *Scutalus tupacii* is sister group of *Bostryx stelzneri* (node 14).

In the third analysis performed using a combined sperm + anatomy and shell character matrix, a single resolved tree was obtained (Fig. 9). Here, Helicoidea is a monophyletic clade (node 13, Bremer support score = 2) and sister group of Orthalicidae (node 17, Bremer support score = 1), which also form a monophyletic clade supported by a sperm synapomorphy (acrosomal pedestal substructure consisting in strations [4(1)]. Synapomorphies supporting helicoidean clade are the sperm nucleus length [1(8.1)], and two other from the genital system, presence of accessory glands [27(1)] and presence of a dart sac in terminal genitalia [34(1)]. Within Orthalicidae, Odontostominae and Bulimulinae are monophyletic. The monophyly of Odontostominae (node 20, Bremer support score = 3) is sustained by four sperm synapomorphies (same as in sperm-based hypothesis) and five other anatomical and shell synapomorphies (characters 18, 21, 23, 26, and 31). The monophyly of Bulimulinae (node 16) is supported by two anatomical + shell synapomorphies (characters 19, 24). Bremer support score for Bulimulinae (0.7) is low. *Drymaeus poecilus* and

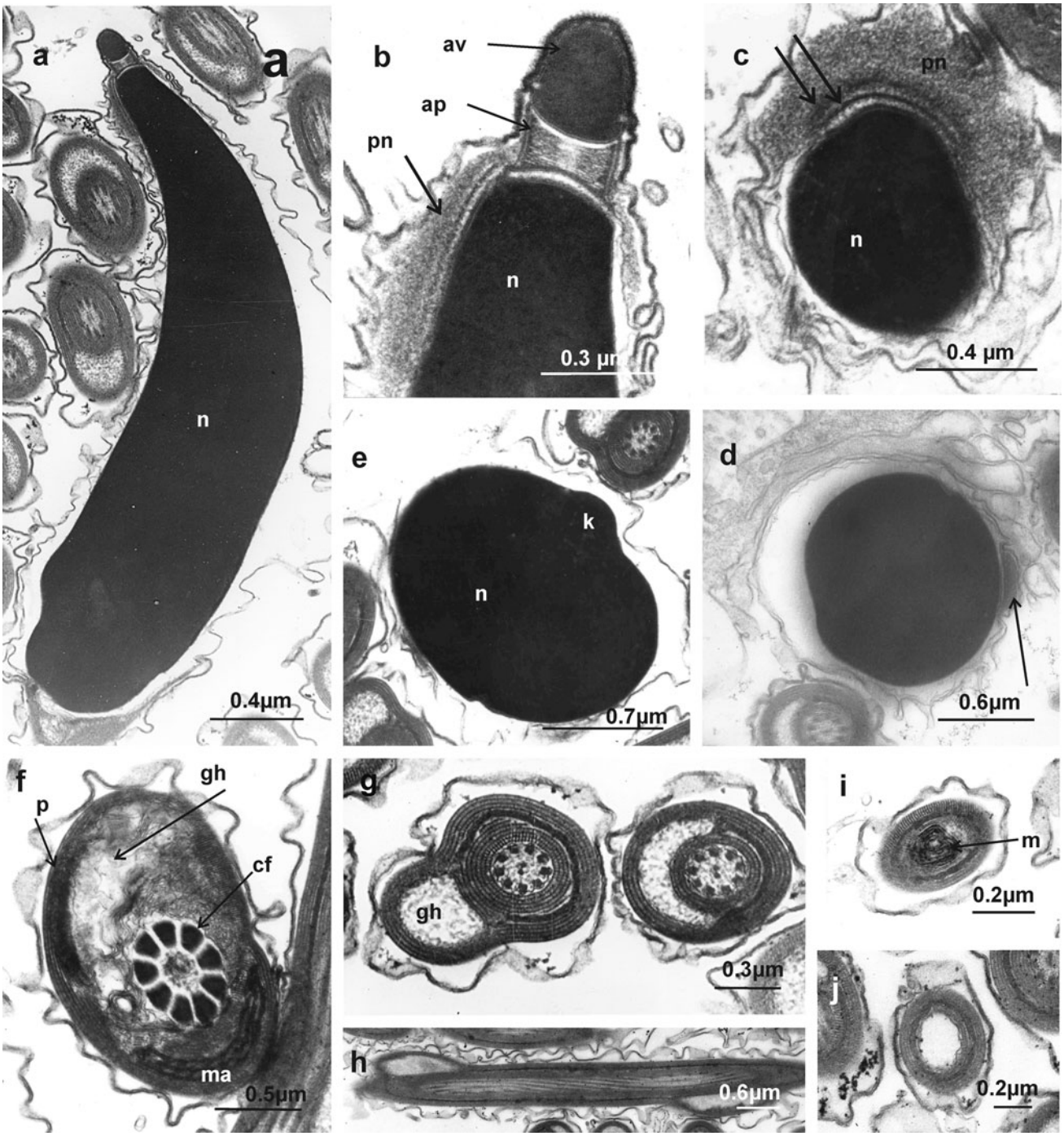

Fig. 5 *Plagiodontes daedaleus*, **a** Longitudinal section (LS) of a sperm head showing acrosomal complex and nucleus shape. **b** Detail of nuclear apex with acrosomal complex. Note the fine transversal striations with the electron-lucent central area of the acrosomal pedestal. The perinuclear sheath is overlapping a short extension of the nuclear apex. **c** Transversal section (TS) of nuclear tip showing the perinuclear sheath with its inner electron-dense layers marked with two arrows. **d** Posterior TS of nucleus. *Arrow* indicates distal portion of perinuclear sheath. **e** TS of nucleus in its basal portion close to implantation fossa. Note the keel. **f** TS of midpiece close to the junction with nucleus. Note the presence of three layers of matrix material of mitochondrial derivative ensheathing the axoneme together with the paracrystalline layers. **g** Posterior TS of midpiece showing only one layer of matrix material of the mitochondrial derivative. Paracrystalline material is traversed by glycogen helix. **h** LS of midpiece showing glycogen helix. **i–j** Terminal TS of midpiece where the axoneme has been replaced by membranous deposits and later an empty space. *av* acrosomal vesicle, *ap* acrosomal pedestal, *cf* coarse fibers, *gh* glycogen helix, *k* nuclear keel, *m* membranous deposits, *ma* matrix material, *p* paracrystalline material of mitochondrial derivative, *n* nucleus, and *pn* perinuclear sheath

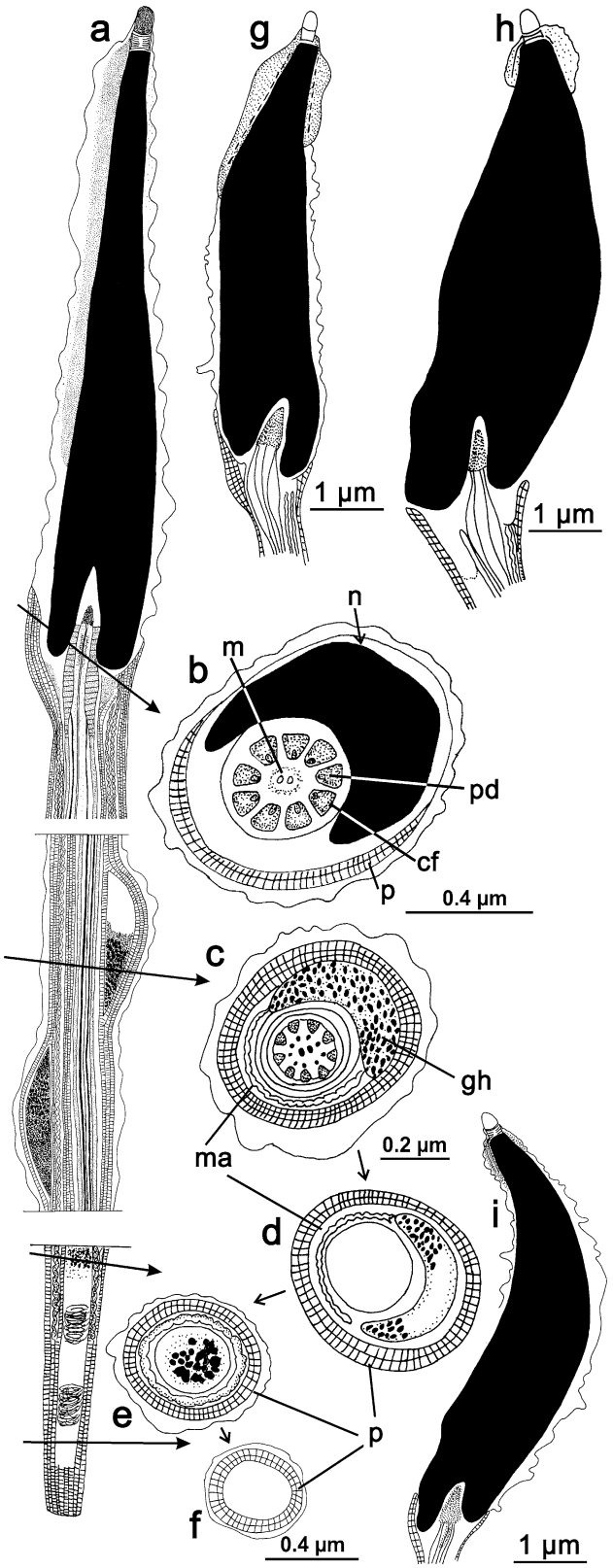

◀ **Fig. 6** Diagram summarizing comparative sperm ultrastructure in the three studied species of Odontostominae and one representing Bulimulinae. **a** Longitudinal sections of head, midpiece, and terminal portion of sperm in *Drymaeus hygrohylaeus.* **b** Semi-transverse section of neck zone of sperm. Note that the peripheral doublets of the axoneme are embedded and masked by the coarse fibers at this midpiece level. **c** Transverse section (TS) of midpiece level with glycogen helix. Coarse fibers and emergent axonemal doublets are surrounded by matrix material and paracrystalline material of the mitochondrial derivative. **d** TS of midpiece without axoneme. The terminal portion of the midpiece begins with the loss of the two central axonemal tubules and coarse fibers. **e–f** TS of terminal portion of sperm at different levels. **g** Longitudinal section (LS) of *Spixia tucumanensis* sperm head. **h** LS of *Clessinia pagoda* sperm head. **i** LS of *Plagiodontes daedaleus* sperm head. *cf* coarse fibers, *gh* glycogen helix, *m* central microtubules of the axoneme, *ma* matrix material of the mitochondrial derivative, *n* nucleus, *p* paracrystalline mitochondrial derivative, and *pd* peripheral axonemal doublets

Drymaeus hygrohylaeus form a clade with 1.4 of Bremer support value, and this clade is sister group of *Bostryx stelzneri.*

Discussion

Sperm morphology is an important source of information for clarifying evolutionary studies on the origin of the Heterobranchia and the relationships among its superfamilies (Healy 1993; Ponder and Lindberg 1997; Dayrat and Tillier 2002). However, from a total of 104 existing taxa traditionally classified as families among the clades Systellommatophora and Stylommatophora (Bouchet and Rocroi 2005), information existing on sperm ultrastructure is restricted only to 14 of these taxa (five of them classified among Helicoidea). Comparisons are difficult to achieve among stylommatophoran sperms, because the level of available information is unequal. Therefore, more studies focusing on the sperm ultrastructure on species of non-helicoidean taxa are urgently needed.

Comparison with other species of Stylommatophora

Sperm of Orthalicidae possess all the characteristic features of pulmonate spermatozoa, like an acrosome composed of an apical vesicle and an acrosomal pedestal, a helically shaped nucleus, and a midpiece, as well as complex mitochondrial derivative forming a continuous sheath with axoneme associated to nine coarse fibers. The presence of a perinuclear sheath, however, seems to be unique among stylommatophoran sperms (Healy 2001). One of the most interesting aspects of the Orthalicidae spermatozoa reported herein is the ultrastructure of the acrosomal complex. A characteristic transverse fine striation in the cylindrical acrosomal pedestal is present in all species studied, except for *Spixia tucumanensis*. A similar acrosomal pedestal has been previously reported in another orthalicid species, *Scutalus tupacii* (Cuezzo 1995). In the remaining stylommatophoran species, the acrosomal pedestal has been described as a cylindrical or conical structure composed of

granular material. The striations present in the acrosome of orthalicid sperms are irregular, parallel to each other but not arranged in regular layers as in the case of nudibrachs *Glossodoris pallida* (Ruppel and Leuckart, 1828) and *Hypselodoris obscura* (Stimpson, 1855) (Wilson and Healy 2002). Coarsely banded acrosomal pedestals have been reported for some Gymnodoridae and Polyceridae nudibranchs species (Healy and Willan 1991). In the remaining stylommatophoran species, the acrosomal pedestal is composed of granular material.

A perinuclear sheath associated with the acrosomal complex and proximal portion of nucleus is reported here for all Orthalicidae species studied. The substructure and thickness of the perinuclear sheath are very peculiar in the Odontostominae species analyzed in having a single or double internal layer of electron-dense material within the granular perinuclear sheath. In Bulimulinae species of *Drymaeus, Bostryx* (this study), and *Scutalus* (Cuezzo 1995), the perinuclear sheath is granular, moderately electron-dense and thinner than in Odontostominae. Simpler perinuclear sheaths, formed by an homogeneous single layer of granular material, have been previously reported for *Cornu aspersum, Helix pomatia* Linnaeus, 1758 (Healy and Jamieson 1989), and *Epiphragmophora tucumanensis* (Doering, 1874) (Cuezzo 1994), while no perinuclear sheath was reported for *Phyllocaulis soleiformis* (Lanza and Quattrini 1964), *Agriolimax reticulatus* (Müller, 1774)(Bayne 1970), *Trichia hispida* (Linnaeus, 1758), and *Succinea putris* (Linnaeus, 1758) (Shileiko and Danilova 1979). In *Oxyloma elegans* (Risso, 1826) (Succineidae), Selmi et al. (1989) described a layer, called paracrystalline body, that lies beneath the acrosomal pedestal around the apex of the nucleus. We regard this layer as homologous to the perinuclear sheath, because of its position surrounding the nucleus. The perinuclear sheath in *Oxyloma elegans* has a paracrystalline ultrastructure contrary to the granular ultrastructure usually described for other pulmonate species. In *Arianta arbustorum* (Linnaeus, 1758), a perinuclear sheath composed of three layers of granular material enclosing the nuclear apex have been described by Bojat et al. (2001). According to them, the perinuclear sheath in the same species vanishes in the spermatheca, and the acrosome is almost aligned with the nuclear axis. Healy and Jamieson (1989) observed no significant ultrastructural differences between spermatozoa taken from the hermaphroditic duct and spermatophores in *Cornu aspersum* and *Helix pomatia*. Morphological changes between the sperm stored in the seminal vesicles and the spermatheca are expected to occur, and these changes can probably be associated with fertilization events. The perinuclear sheath was not reported to be present in species of Systellommatophora investigated (Lanza and Quattrini 1964; Healy 1986; Selmi et al. 1988). The acrosomal complex in stylommatophoran sperms can be slightly tilted in relation to the longitudinal axis of the sperm (Healy and Jamieson 1989; Cuezzo 1995; Bojat et al. 2001) or maximally reflected backwards from the nuclear apex as in *Cornu aspersum* (Healy and Jamieson 1989). In orthalicid sperms, the tilted acrosomal complex has been observed to be present in some specimens of *Drymaeus, Scutalus* (Cuezzo 1995), and *Plagiodontes*, while in the other species, the acrosomal pedestal was always found axially aligned. It has been suggested that this morphological rearrangement of the acrosomal complex takes place in the hermaphroditic duct since sperms and late spermatids in the ovotestis are always axially aligned (Healy 2001).

Sperm nucleus in orthalicid species examined is helical, and keels are slightly pronounced except in Odontostominae where keels are more pronounced at the base of the nucleus. Within Stylommatophora, there is a tendency to have nuclei with keels slightly prominent as the ones present in Helicoidea (Giusti et al. 1991), while in basommatophoran snails, nuclear keels are usually heavily pronounced (Healy 1983). The presence of a subnuclear ring in *Drymaeus, Bostryx*, and *Clessinia* species is also noteworthy because this structure was previously assumed to be absent in stylommatophoran sperms (Giusti et al. 1991). Although not described in the text, a subnuclear ring was drawn in a figure representing the sperm of *Succinea putris* by Shileiko and Danilova (1979). The terminal portion of Orthalicidae sperms, as it is the case of stylommatophoran sperms, lack a glycogen piece and annulus and the axoneme ends before the mitochondrial derivative. Along the midpiece, the size and shape of the single glycogen helix decrease considerably, reducing gradually its contents of glycogen-like granules until the helix disappears. The midpiece of *Succinea putris* sperms (Succineidae) is traversed by three helices (Shileiko and Danilova 1979). More than one glycogen helix in the midpiece has been also described for species of Hygrophila (Thompson 1973; Maxwell 1975; Kitajima and Paraense 1976; Rigby 1982; Healy 1983, 1988) and Veronicellidae (Lanza and Quattrini 1964), and up to four glycogen helices have been reported in some cephalaspid opisthobranch species (Wilson and Healy 2002).

Phylogenetic implications

Although sperm ultrastructure of only six species of Orthalicidae have been examined here *(Spixia tucumanensis, Plagiodontes daedaleus, Clessinia pagoda, Drymaeus hygrohylaeus, D. poecilus*, and *Bostryx stelzneri*), the data available are of importance because sperm unambiguous synapomorphies have been identified, supporting the monophyly of some clades in the cladistic analyses performed.

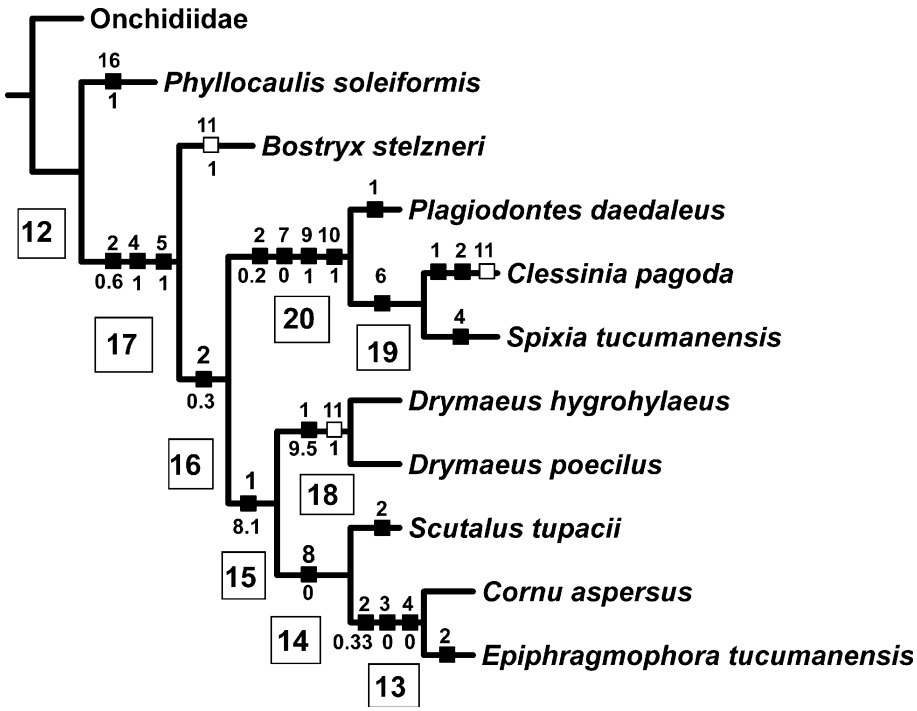

Fig. 7 Most parsimonious tree obtained with sperm-based character matrix (Table 2, 1–16 characters). Node numbers are located below *branches* inside *squares*. Unambiguous synapomorphies are indicated with *black hash marks* on each branch; character numbers are above *hash marks* and character state below *hash marks*

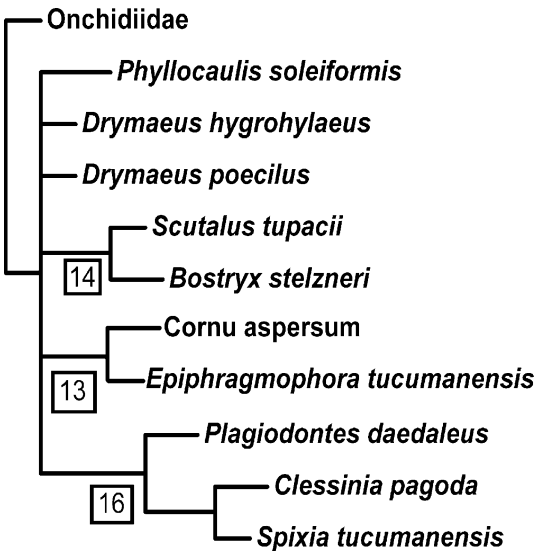

Fig. 8 Strict consensus tree from four original trees obtained with the anatomy + shell character-based matrix (Table 2, 17–34 characters). Node numbers are located below *branches* inside *squares*

Orthalicidae is supported as a monophyletic group in the sperm + anatomy-based cladogram. One unambiguous sperm synapomorphy, the acrosomal pedestal substructure, sustained this clade. In the sperm-based cladogram, the helicoidean species are merged within the Bulimulinae species due to their similarities in nucleus length and shape, especially with *Drymaeus* sperms. However, when other anatomical characters were included in the analysis, the Helicoidea clearly constitutes a different clade. The helicoidean clade represented by *Epiphragmophora tucumanensis* and *Cornu aspersum* is monophyletic and supported by features of the acrosomal complex in all analyses performed. Within Orthalicidae, Bulimulinae is a paraphyletic group as it was stated by previous cladistic analyses based on a more complete morphological matrix (Cuezzo et al. 2010) or on molecular studies (Breure et al. 2010). However, in the combined sperm + anatomy-based cladogram, Bulimulinae appears as a monophyletic clade with a low Bremer support score [0.7] due to the restricted taxa selection used that constitutes by itself a monophyletic clade within the group (Breure et al. 2010). *Drymaeus* and *Bostryx* sperms have nuclei markedly reduced in twisting, slender and longer, with acrosomal pedestals cylindrical and slightly higher than the rest of species from different genera investigated. The nuclear length in *Drymaeus hygrohylaeus* (9.6 μm) is only comparable with the one reported for *Helix pomatia* (10 μm) (Healy and Jamieson 1989) and *Anguispira alternata* (13 μm) (Atkinson 1982) since the rest of the stylommatophoran nuclei sperm length range between 5 and 8 μm. *Drymaeus* sperm is clearly differentiated from helicids sperms for the acrosomal pedestal substructure and presence of a subnuclear ring.

Odontostominae forms a monophyletic clade with strong Bremer support score in the three cladistic analyses performed. The shallow acrosomal pedestals (01–02 μm), thick perinuclear sheath, strong and short nuclei with basal keels are autapomorphies that support the monophyly of Odontostominae. The highly electron-dense substructure of the perinuclear sheath (character 6) represent a

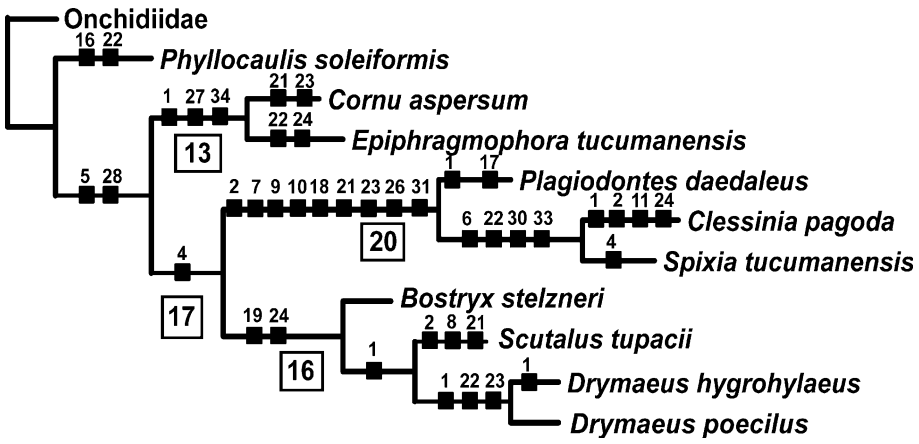

Fig. 9 Most parsimonious tree obtained with combined sperm + anatomical + shell character matrix. Node numbers are located below branches inside *squares*. Unambiguous synapomorphies are indicated with *black hash marks* on each branch, and character numbers are above *hash marks*

synapomorphy of the sister group formed by *Spixia tucumanensis* and *Clessinia pagoda.* The phylogenetic relationships among the three genera involved are congruent in both analyses performed. These relationships are also supported by sperm synapomorphies. Finally, when analyzing all the characters together (Fig. 9), the effect of sperm characters in the topology of the tree obtained is evident. The groups well supported as it is the case of Odontostominae, and Helicoidea did not change but received extra support. The position of Helicoidea, with the addition of anatomical characters, was substantially changed in the combined phylogeny in comparison with the sperm-based cladogram. Sperm + anatomy-based hypothesis support a sister relationship of Orthalicidae with Helicoidea, relationship previously proposed by Barker (2001) phylogenetic hypothesis. In another case, a sperm synapomorphy supported the monophyly of the whole Orthalicidae (Fig. 9) that it was not resolved in the anatomy-based cladogram (Fig. 8). It is worth noting that the monophyly of Helicoidea and Odontostominae was recovered in all analysis performed.

The present study and cladistic analyses performed suggest that characters on sperm ultra structure are informative for stylommatophoran systematic and phylogenetic approaches. Within Orthalicidae sperm, characters provided synapomorphies at familiar, subfamiliar, and generic level that gave extra support to the relationships obtained.

Acknowledgments Staff of the Laboratory of Electron Microscopy of Northwestern Argentina (LAMENOA) is greatly acknowledged for the support given to the present study. JM Healy is thanked for kindly providing information and special literature that made this study possible. A. Gandolfo Nixon (Cornell University, USA) and S. Toranzo are thanked for reviewing English language. The author is grateful to the editor, Th. Bartolomaeus, and anonymous reviewers for their detailed review and suggestions. Permission for collecting specimens was provided by the Argentinean National Park Service Agency to which the author's gratitude is extended. The author is a researcher of CONICET (Consejo Nacional de Investigaciones Científicas y Técnicas, Argentina), support from which is greatly acknowledged. Funding to develop this research was provided by PIP 6048 (CONICET) and PICT 528 (ANPCyT).

References

Anderson WA, Personne P (1967) The fine structure of the neck region of the spermatozoa of *Helix aspersa*. J Microscopie 6:1033–1042

Anderson WA, Personne P (1969a) Structure and histochemistry of the basal body derivative, neck and axoneme of spermatozoa of *Helix aspersa*. J Microscopie 8:87–96

Anderson WA, Personne P (1969b) The cytochemical localization of sorbitol dehydrogenase activity in spermatozoa of *Helix aspersa*. J Microscopie 8:97–102

Anderson WA, Personne P (1970) The localization of glycogen in the spermatozoa of various invertebrate and vertebrate species. J Cell Biol 44:29–51

Anderson WA, Personne P, André J (1968) Chemical compartmentalization in *Helix* spermatozoa. J Microsc 7:367–390

Atkinson JW (1982) An ultrastructural analysis of the mature spermatozoa of *Anguispira alternata* (Say) (Pulmonata, Stylommatophora). J Morphol 173:249–257

Barker GM (2001) Gastropods on land: phylogeny, diversity and adaptative morphology. In: Barker GM (ed) The biology of terrestrial Molluscs. CABI Publishing, Wallingford, pp 1–146

Bayne CJ (1970) Organization of the spermatozoon of *Agriolimax reticulatus*, the grey field slug (Pulmonata: Stylommatophora). Z Zellforsch Mikrosk Anat 103:75–89

Bojat NC, Sauder U, Hasse M (2001) The spermathecal epithelium, sperm and their interactions in the hermaphroditic land snail *Arianta arbustorum* (Pulmonata, Stylommatophora). Zoomorphology 120:149–157

Bouchet P, Rocroi JP (2005) Classification and nomenclator of gastropod families. Malacologia 47:1–397

Bremer K (1988) The limit of amino-acid sequence data in angiosperm phylogenetic reconstruction. Evolution 42:795–803

Bremer K (1994) Branch support and tree stability. Cladistics 10:295–304

Breure A (1979) Systematics, phylogeny and zoogeography of Bulimulinae (Mollusca). Zool Verh 168:1–100

Breure ASH, Groenenberg D, Schilthuizen M (2010) Gondwana revisited: new insights in the phylogenetic relationships within Orthalicoidea. In: Actas VI Southern connection congress. p 35

Cuezzo MG (1994) Ultrastructure of the mature spermatozoa of the land snail *Epiphragmophora tucumanensis* (Doering, 1874) (Gastropoda: Helicoidea). J Moll Stud 61:1–7

Cuezzo MG (1995) Spermatogenesis and sperm structure in the Neotropical Pulmonate snail *Scutalus tupacii* (d'Orbigny). Veliger 38:212–222

Cuezzo MG (2006) Systematic revision and cladistic analysis of *Epiphragmophora* Doering from Argentina and southern Bolivia (Gastropoda: Stylommatophora). Malacologia 49:121–188

Cuezzo MG, Valdovinos C, Breure ASH (2010) *Discoleus* Breure, 1978: is there a pre-Gondwanan ancient stock of Orthalicidae? (Mollusca, Stylommatophora). In: Actas VI Southern connection congress. p 34

Dan JC, Takaichi S (1979) Spermiogenesis in the Pulmonate snail, *Euhadra hickonis* III. Flagelum formation. Dev Growth Differ 21:71–86

Dayrat B (2010) Comparative anatomy and taxonomy of *Onchidium vaigiense* (Gastropoda: Pulmonata: Onchidiidae). Molluscan Res 30:87–101

Dayrat B, Tillier S (2002) Evolutionary relationships of euthyneuran gastropods (Mollusca): a cladistic re-evaluation of morphological characters. Zool J Linn Soc 135:403–470

Franzén A (1955) Comparative morphological investigations into the spermiogenesis among Mollusca. Zool Bidr Uppsala 30:399–456

Giusti F, Manganelli G, Selmi G (1991) Spermatozoon fine structure in the phylogenetic study of the Helicoidea (Gastropoda, Pulmonata). In: Meier-Brook C (ed) Proceedings of the tenth international malacological congress. Unitas Malacologica, Tübingen, pp 611–616

Goloboff P, Farris J, Nixon K (2008) TNT, a free program for phylogenetic analysis. Cladistics 24:774–786

Healy JM (1983) An ultrastructural study of Basommatophoran spermatozoa (Mollusca, Gastropoda). Zool Scr 12:57–66

Healy JM (1986) Electron microscopic observations on the spermatozoa of a marine "pulmonate" slug, *Onchidium damellii* (Gastropoda, Onchidiacea). J Submicrosc Citol 18:587–594

Healy JM (1988) Sperm morphology and its systematic importance in the Gastropoda. Malacol Rev 4:251–266

Healy JM (1993) Comparative sperm ultrastructure and spermiogenesis in basal heterobranch gastropods (Valvatoidea, Architectonicoidea, Rissoelloidea, Omalogyroidea, Pyramidelloidea) (Mollusca). Zool Scr 22:263–276

Healy JM (1996) Molluscan sperm ultrastructure: correlation with taxonomic units within the Gastropoda, Cephalopoda and Bivalvia. In: Taylor J (ed) Origin and evolutionary radiation of the Mollusca. Oxford University Press, Oxford, pp 99–113

Healy JM (2001) Spermatogenesis and oogenesis. In: Barker GM (ed) The biology of terrestrial Molluscs. CABI Publishing, Wallingford, pp 357–382

Healy JM, Jamieson BGM (1989) An ultrastructural study of spermatozoa of *Helix aspersa* and *Helix pomatia* (Gastropoda, Pulmonata). J Moll Stud 55:389–404

Healy JM, Willan RC (1991) Nudibranch spermatozoa: comparative ultrastructure and systematic importance. Veliger 34:134–165

Karnovsky MJ (1965) A formaldehyde-glutaraldehyde fixative of high osmolality for use in electron microscopy. J Cell Biol 27:137–138

Kitajima EW, Paraense WL (1976) The ultrastructure of mature sperms of the fresh water snail *Biomphalaria glabrata* (Mollusca, Gastropoda). Trans Am Microsc Soc 95:1–10

Lanza B, Quattrini D (1964) Osservazioni sulla spermiogenesi e sugli spermi di *Vaginulus borellianus* (Coloso) (Gastropoda, Soleolifera). Bol Zool 31:1322–1338

Maxwell WL (1975) Scanning electron microscope studies of Pulmonate spermatozoa. Veliger 18:31–33

Maxwell WL (1976) The neck region of the spermatozoon of *Discus rotundatus* (Müller) (Pulmonate, Stylommatophora). J Morphol 150:299–306

Maxwell WL (1983) Mollusca. In: Adiyodi KG, Adiyodi RG (eds) Reproductive biology of invertebrates II. Spermatogenesis and sperm function. Wiley, Chichester, pp 275–319

Miquel SE (1993) Las especies del género *Bostryx* Troschel 1847 (Gastropoda, Stylommatophora, Bulimulidae) en la Republica Argentina (1er parte). Arch Moll 121:157–171

Miquel SE (1995) Las especies del género *Bostryx* Troschel 1847 (Gastropoda, Stylommatophora, Bulimulidae) en la Republica Argentina (2da parte). Arch Moll 124:119–127

Nixon K (1999) WINCLADA. Character analysis program. Published by the author

Odiete WO (1982) Fine structural studies on the ovotestis of *Archachatina marginata* (Swainson) (Pulmonata, Stylommatophora). Malacologia 22:137–143

Parodiz JJ (1942a) Los Odontostominos en Argentina, Primera parte. Physis 19:191–218

Parodiz JJ (1942b) Los Odontostominos en Argentina, Segunda parte. Physis 19:319–343

Parodiz JJ (1946) Los géneros de Bulimulinae argentinos. Rev Mus La Plata Zool 4:303–371

Pizá J (2008) Variabilidad morfométrica, anatomía interna y distribución geográfica del género *Plagiodontes* (Gastropoda, Odontostominae). Dissertation, Universidad Nacional del Sur, Buenos Aires, Argentina

Ponder WF, Lindberg DR (1997) Towards a phylogeny of gastropod mollusks: an analysis using morphological characters. Zool J Linn Soc 119:83–265

Quattrini D, Lanza D (1965) Ricerche sulla biologia dei Veronicellidae (Gastropoda, Soleolifera). Struttura della gonade, ovogenesi e spermatogenesis in *Vaginulus borellianus* (Colosi) e in *Laevicaulis alte* (Ferussac). Monit Zool 73:1–60

Reger JF, Fitzgerald MEC (1982) Studies on the fine structure of the mitochondrial derivative in spermatozoa of a Gastropod. Tissue Cell 14:775–783

Rigby JE (1982) The fine structure of differentiating spermatozoa and sertoli cells in the gonad of the pond snail, *Lymnaea stagnalis*. J Moll Stud 48:111–123

Rodrigues Gomes S (2007) Filogenia morfológica de Veronicellidae, filogenia molecular de *Phyllocaulis* Colosi e descrição de uma nova espécie para a família (Mollusca, Gastropoda, Pulmonata). PhD dissertation, Universidade federal do Rio Grande do Sul, Porto Alegre, Brazil

Salas Oroño E (2007) Taxonomic review of the *Spixia pyriformis* species complex (Mollusca, Gastropoda, Odontostominae). Zootaxa 1498:1–25

Selmi MG, Giusti F, Manganelli G (1988) The fine structure of the mature spermatozoon of *Onchidella caltica* (Cuvier) (Mollusca: Gastropoda) and its phylogenetic implications. J Ultrastruct Mol Struct Res 99:107–123

Selmi MG, Bigliardi E, Giusti F (1989) Morphological modifications in stored Heterospermatozoa of *Oxyloma elegans* (Pulmonata: Stylommatophora). J Ultrastruct Mol Struct Res 102:82–86

Sereno P (2007) Logical basis for morphological characters in phylogenetics. Cladistics 23:565–587

Shileiko LV, Danilova LV (1979) Ultrastructure of spermatozoa in Pulmonate Molluscs *Trichia hispida* and *Succinea putris*. Sov J Dev Biol 10:392–401

Takaichi S (1975) The fine structure of spermatozoa of *Euhadra hickonis*. Zool Mag 84:48–57

Takaichi S (1978) Spermiogenesis in the Pulmonate snail, *Euhadra hickonis.* II Structural changes of the nucleus. Dev Growth Differ 20:301–315

Takaichi S, Dan JC (1977) Spermiogenesis in the Pulmonate snail *Euhadra hickonis.* I. Acrosome formation. Dev Growth Differ 19:1–14

Takaichi S, Sawada N (1973) An electron microscope study on sperm formation in *Euhadra hickonis*. Mem Ehime Univ 7:17–34

Thompson TE (1973) Euthyneuran and other Molluscan spermatozoa. Malacologia 14:167–206

Whitehead SI, Hodgson AN (1985) A study of the spermatozoa and spermatogenesis of the giant snail *Achatina zebra*. Proc Electron Microsc Soc South Afr 15:193–194

Wilson NG, Healy JM (2002) Comparative sperm ultrastructure in five genera of the Nudibranch family Chromodoridae (Gastropoda, Opisthobranchia). J Moll Stud 68:133–145